

Global Estimates of Fine Particulate Matter using a Combined Geophysical-Statistical Method with Information from Satellites, Models, and Monitors

Aaron van Donkelaar,^{*,†} Randall V. Martin,^{†,‡} Michael Brauer,[§] N. Christina Hsu,^{||} Ralph A. Kahn,^{||} Robert C. Levy,^{||} Alexei Lyapustin,^{||,⊥} Andrew M. Sayer,^{||,⊥} and David M. Winker[#]

[†]Department of Physics and Atmospheric Science, Dalhousie University, Halifax, N.S. Canada

[‡]Harvard-Smithsonian Center for Astrophysics, Cambridge, Massachusetts 02138, United States

[§]School of Population and Public Health, The University of British Columbia, 2206 East Mall, Vancouver, British Columbia V6T1Z3, Canada

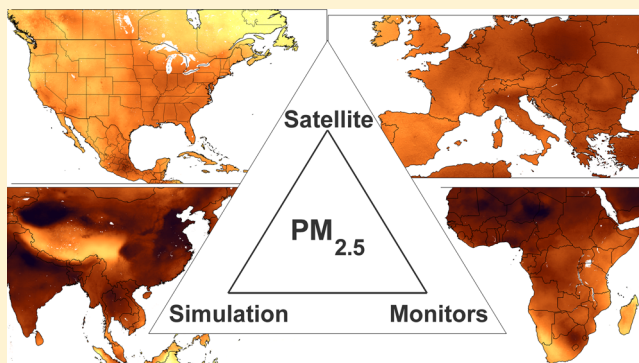
^{||}NASA Goddard Space Flight Center, Greenbelt, Maryland 20771, United States

[⊥]Goddard Earth Sciences Technology and Research, Universities Space Research Association, Greenbelt, Maryland 20771, United States

[#]NASA Langley Research Center, Hampton, Virginia 23665, United States

S Supporting Information

ABSTRACT: We estimated global fine particulate matter (PM_{2.5}) concentrations using information from satellite-, simulation- and monitor-based sources by applying a Geographically Weighted Regression (GWR) to global geophysically based satellite-derived PM_{2.5} estimates. Aerosol optical depth from multiple satellite products (MISR, MODIS Dark Target, MODIS and SeaWiFS Deep Blue, and MODIS MAIAC) was combined with simulation (GEOS-Chem) based upon their relative uncertainties as determined using ground-based sun photometer (AERONET) observations for 1998–2014. The GWR predictors included simulated aerosol composition and land use information. The resultant PM_{2.5} estimates were highly consistent ($R^2 = 0.81$) with out-of-sample cross-validated PM_{2.5} concentrations from monitors. The global population-weighted annual average PM_{2.5} concentrations were 3-fold higher than the 10 $\mu\text{g}/\text{m}^3$ WHO guideline, driven by exposures in Asian and African regions. Estimates in regions with high contributions from mineral dust were associated with higher uncertainty, resulting from both sparse ground-based monitoring, and challenging conditions for retrieval and simulation. This approach demonstrates that the addition of even sparse ground-based measurements to more globally continuous PM_{2.5} data sources can yield valuable improvements to PM_{2.5} characterization on a global scale.



1. INTRODUCTION

Ambient fine particulate matter (PM_{2.5}) concentrations contribute significantly to global disease burden, causing 3 million premature deaths in 2013.¹ Satellite observations, simulations, and ground monitors provide insight into global PM_{2.5} exposure, but availability and quality of these data sources vary regionally. Exposure assignments, such as for the Global Burden of Disease² (GBD), would benefit from more sophisticated methods to combine these sources into a unified best-estimate. Geophysical relationships between aerosol optical depth (AOD) and PM_{2.5} simulated using chemical transport models (CTM) have allowed surface PM_{2.5} to be globally estimated from satellite AOD observations,³ but underutilize the insight that ground-based monitors can provide. Statistical methods, such as Land Use Regression

and Geographically Weighted Regression (GWR), have been effective at combining the spatial coverage of satellite observations with the accuracy of ground-based monitors where monitor density is high, such as in North America,⁴ China,⁵ and Europe.⁶ The global paucity of ground-based monitors has traditionally restricted application of these methods on a larger scale.

Major advances in satellite remote sensing include new retrieval algorithms with high accuracy, long-term stability, and high resolution.^{7–13} The ground-based AERONET sun

Received: November 26, 2015

Revised: February 29, 2016

Accepted: March 8, 2016

Published: March 8, 2016

photometer network¹⁴ offers long-term globally distributed AOD measurements that provide insight into the relative skill of these retrieval algorithms. A method has been demonstrated of combining geophysical satellite-derived PM_{2.5} estimates with GWR over North America to draw on the strengths of all three PM_{2.5} information sources; this approach retained consistent agreement ($R^2 = 0.78$) at cross-validation sites even when 70% of sites were withheld, suggesting this approach might be extended to regions with only sparse PM_{2.5} monitoring.¹⁵

Here we present and evaluate a global framework based on that combined approach. We evaluate the retrieved and simulated total column AOD from numerous sources using AERONET to produce a globally continuous AOD field based on the relative uncertainty of each source. We relate AOD to PM_{2.5} geophysically, using their simulated relationship in combination with the CALIOP space-borne lidar.¹⁶ Globally distributed, ground-based monitors are used to predict and account for the residual bias in the combined PM_{2.5} estimates through GWR, and the results are tested for independence. This work represents a step forward in both understanding sources of bias associated with satellite-derived PM_{2.5} estimates, as well as a major improvement in characterization of global PM_{2.5} concentrations.

2. SOURCES OF INFORMATION: INSTRUMENTATION, RETRIEVAL ALGORITHMS, AND SIMULATION

Passive Satellite Instruments. We used AOD retrieved from four “passive” satellite instruments that observe back-scattered solar radiation.

Twin Moderate resolution Imaging Spectroradiometer (MODIS) instruments reside onboard the polar-orbiting Terra and Aqua satellites, launched in 2000 and 2002, respectively. With a broad swath width of 2330 km, each instrument provides near-global daily coverage at 36 spectral bands between 0.412 and 14.5 μm with a nadir spatial resolution of 250 m to 1 km, depending on spectral channel. The MODIS Collection 6 release improves the calibration to correct for sensor degradation, allowing more consistent retrievals throughout their lifetime to date.¹⁷

The Multiangle Imaging SpectroRadiometer (MISR) instrument, also onboard the Terra satellite, provides nine views of each 275 m to 1.1 km nadir resolution pixel, at angles ranging from nadir to 70.5° fore and aft in four spectral bands between 0.446 and 0.866 μm . The MISR instrument swath width of ~380 km takes about a week for complete global coverage at midlatitudes, and has demonstrated spectral stability throughout its lifetime.^{18,19}

The Sea-viewing Wide Field-of-view Sensor (SeaWiFS) instrument was operational from 1997 to 2010. SeaWiFS' 1500 km swath provided near-daily global observation in 8 spectral bands between 0.402 and 0.885 μm with a nadir spatial resolution of 1.1 km. The radiometric calibration of SeaWiFS was stable over its lifetime.²⁰

Passive Retrieval Algorithms. Several AOD retrieval algorithms have been developed from top-of-atmosphere reflectances observed by these instruments over various surfaces. Individual algorithms can excel under certain conditions, or alternatively provide similar quality under others.^{21,22}

The Collection 6 Dark Target (DT) retrieval algorithm over land⁷ relates surface reflectances observed at near-infrared wavelengths, where aerosol scattering effects are reduced, to visible wavelengths using NDVI-based relationships to represent underlying vegetation and other surface types.⁸

Observed top-of-atmosphere reflectances over dark surfaces are corrected for absorption by atmospheric gases and related to AOD, accounting for the effects of aerosol and molecular scattering. We used 10 km resolution DT applied to MODIS instruments.

The Deep Blue (DB) algorithm was initially developed for MODIS AOD retrieval over bright surfaces, such as deserts.¹⁰ DB utilizes blue wavelengths, where reduced surface reflectance allows greater sensitivity to AOD. DB has been enhanced since its inception to include polarization effects, dynamic and geolocated surface reflectance, and extended to “dark” land surfaces.⁹ DB is applied to SeaWiFS²³ at 13.5 km resolution and to MODIS at 10 km resolution.

The Multi-Angle Implementation of Atmospheric Correction (MAIAC) retrieval algorithm uses time series analysis and image processing to derive the surface bidirectional reflectance function at fine spatial resolution.^{11,12} Multiple, single-view passes are combined over up to 16 days to exploit multiangle viewing effects. MAIAC uses empirically tuned, regionally prescribed, aerosol properties following the AERONET climatology, and provides AOD at 1 km spatial resolution over land globally from MODIS. MAIAC was not globally available at the time of this work, but will be in the future.

The MISR retrieval algorithm (v22)²⁴ uses same-scene multiangular views to simultaneously solve for surface and atmospheric top-of-atmosphere reflectance contributions, providing AOD retrievals over land without absolute surface reflectance assumption. MISR retrieves over both dark and bright surfaces. MISR retrievals use multiple aerosol models with different refractive index, particle size and shape (nonsphericity), allowing for retrieval of aerosol size and type in many conditions.¹³ MISR retrievals are applied to the MISR instrument at 17.6 km resolution.

CALIOP Satellite Instrument. The “active” Cloud-Aerosol Lidar with Orthogonal Polarization (CALIOP) instrument has provided global vertical aerosol profiles from the Cloud-Aerosol Lidar and Infrared Pathfinder Satellite Observation (CALIPSO) satellite since 2006.¹⁶ CALIOP observes the backscattered radiation from laser pulses it emits at 532 and 1064 nm. Aerosol extinction profiles (v3.01) are retrieved at a resolution of 30 m vertical up to 8 km above the surface, and 5 km horizontal.

GEOS-Chem Chemical Transport Model. We used the GEOS-Chem chemical transport model (<http://geos-chem.org>; v9-01-03) as an additional data source for AOD, and to simulate the spatiotemporally varying geophysical relationship between AOD and PM_{2.5}. Assimilated meteorology from the NASA Goddard Earth Observation System (GEOS) drives the simulations for 2004–2012 (GEOS-5.2) and 1998–2014 (GEOS5.7). Nested GEOS-Chem simulations for North America,^{25,26} Europe²⁷ and East Asia²⁸ used GEOS-5.2 at 0.5° × 0.67° and 47 vertical levels. Our global simulations at 2° × 2.5° used GEOS-5.2 when available and otherwise GEOS-5.7. The use of GEOS-5.2 allowed for higher resolution within the nested regions. Each aerosol type simulated with GEOS-5.7 was scaled by its mean monthly ratio with the GEOS-5.2 driven simulation based on a 2004–2012 overlap period. The top of lowest model layer is approximately 100 m.

The GEOS-Chem aerosol simulation includes sulfate-nitrate-ammonium,^{29,30} primary^{31–33} and secondary carbonaceous aerosols,^{34–36} mineral dust,³⁷ and sea-salt.³⁸ Aerosol optical properties were determined from Mie calculations of log-normal size distributions, growth factors and refractive indices,

based on the Global Aerosol Data Set (GADS) and aircraft measurements.^{39–41} We reduced by half the AOD to $PM_{2.5}$ relationship for mineral dust to compensate for its overly vigorous wet deposition in the simulation.⁴¹ Details of the GEOS-5.2-driven simulation are described in Philip et al.,⁴² and of the GEOS-5.7-driven simulation in Boys et al.⁴³

AERONET. The Aerosol Robotic Network (AERONET) is a globally distributed ground-based network of CIMEL sun photometers¹⁴ that provide multiwavelength AOD measurements. AERONET measurements apply the Beer–Lambert–Bouguer law to observed direct beam radiation to calculate spectral AOD with a low uncertainty of <0.02 ,⁴⁴ making it invaluable for evaluation of both simulated and satellite-retrieved AOD. We used level 2.0 of version 2 data.

Surface Monitors. We used surface monitor $PM_{2.5}$ data collected for the Global Burden of Disease (GBD).² This data set combines multisource, annually representative $PM_{2.5}$ and PM_{10} observations from GBD collaborators, targeted data searches, official networks, literature searches, and the WHO ambient air pollution in cities database. Observations were collected for the years 2008–2013. PM_{10} observations, scaled by nearest available $PM_{2.5}:PM_{10}$ ratios, were used in regions without direct $PM_{2.5}$ measurement as detailed by Brauer et al.²

A summary of the data sources used is given in [Supporting Information Table 1](#).

3. MATERIALS AND METHODS

Common Calibration and Definition of Error. We first globally calibrated each AOD source using AERONET observations. We translated daily AOD retrievals and simulated values from 1998 to 2014 from their native resolution onto a common $0.1^\circ \times 0.1^\circ$ grid, area-weighting satellite retrievals and linearly interpolating simulated values. Daily satellite AOD retrievals were sampled coincidentally to within 0.25° of each AERONET location and binned according to Normalized Difference Vegetation Index (NDVI). NDVI was used to represent the effects of seasonally based changes in vegetation. Ten percent of the data were withheld from each of 100 random draws. Reduced major axis linear regression determined the line of best fit for the remaining data. Median slope and offset of the retrieved or simulated AOD with observed values were treated as local calibration.

Local calibrations were used to create a global surface for application to the AOD sources, where each pixel over the global was determined as the weighted average of all AERONET site-specific calibrations. Weighting factors were represented by the inverse product of Land Cover Similarity (LCS) and distance squared. We defined LCS as

$$LCS_{i,j,k} = \sum_{n=1}^{N_{LT}} |LT_{i,j,n} - LT_{k,n}| \quad (1)$$

where the LCS of a global pixel (i,j) with AERONET site (k) was the sum of absolute differences between land cover type percentages ($LT_{i,j,n}$ and $LT_{k,n}$) for each land cover category (n) as defined by the MODIS land cover product.⁴⁵ Land cover percentages were capped at a maximum of 50% and their absolute difference given a minimum of 1%. LCS allowed similar mixtures of land cover to be weighted more strongly. Example weighting factors of four AERONET locations are shown in [Supporting Information Figure S1](#). The impact of changing land type on weighting factor, often associated with

topographical changes, is visible as deviations from the smooth variation of inverse squared distance.

Residual uncertainty in calibrated AOD was represented by the normalized root-mean-square difference (NRMSD) between coincidentally sampled AOD at AERONET sites after application of the global bias correction surface:

$$NRMSD = \frac{(\text{MEAN}((AOD_{\text{RETRIEVED}} - AOD_{\text{AERONET}})^2))^{0.5}}{AOD_{\text{AERONET}}} \quad (2)$$

Local NRMSD were globally extended using inverse squared distance and LCS, following the approach used for the local calibration factors.

We also calibrated simulated AOD with AERONET measurements. Simulated fractional aerosol composition was applied to each daily AERONET observation and unique calibration terms determined seasonally for each component, following van Donkelaar et al.²⁷ Local calibration terms were extended globally using the inverse squared distance and cross-correlation weighted average of each AERONET site to each global pixel. Calibrated, component-specific residual uncertainty was represented by NRMSD and extended globally also using inverse squared distance and cross-correlation.

CALIOP-Based Vertical Profile Adjustment. We applied CALIOP aerosol extinction vertical profiles (CAL_LID_L2_05kmAPro-Prod-V3-01) to correct the GEOS-Chem simulation of AOD to near-surface extinction. Vertical profile adjustments were determined globally using CALIOP extinction profiles, sampled coincidentally in time and space with simulations over the CALIOP v3.01 period of 2006–2011. CALIOP vertical profiles were adjusted for consistent aerosol optical properties with GEOS-Chem using the lidar equation.²⁷ The effect of optical property differences was generally small. Simulated fractional aerosol composition was applied to the CALIOP profiles, and local vertical profile adjustments determined for each climatological month of each component as the ratio of median CALIOP and simulated near-surface extinction to AOD. A minimum AOD column of 0.01 and near-surface extinction of 0.1 km^{-1} were required. Local adjustments were spatially smoothed using a moving median over a 30° latitude and 45° longitude window.

Estimation of $PM_{2.5}$ from Satellite and Simulation. We related daily calibrated AOD values from each source on a 0.1° grid to near surface $PM_{2.5}$ concentrations using CALIOP-adjusted daily simulated AOD to $PM_{2.5}$ relationships. Filters were applied to exclude AOD and $PM_{2.5}$ outliers from each source. Daily values differing from the local mean (within $1^\circ \times 1^\circ$) by more than the local standard deviation were removed. Values were removed where local standard deviations exceeded twice the local mean. Values were also removed where less than 25% of local retrievals were successful and above zero. Monthly mean AOD and $PM_{2.5}$ surfaces for each source were calculated from these daily values and the same filters applied to the monthly surfaces. $PM_{2.5}$ was treated at 35% relative humidity to match common standardized measurement procedures.

Monthly mean values with less than 50% coverage within the surrounding five degrees were removed. Missing AOD and $PM_{2.5}$ estimates within areas with more than 50% coverage were approximated using the interpolated ratio with the same data source during other years of the same month, or barring that, the interpolated ratio with simulated values during the same time period. Monthly AOD and $PM_{2.5}$ values from all N sources

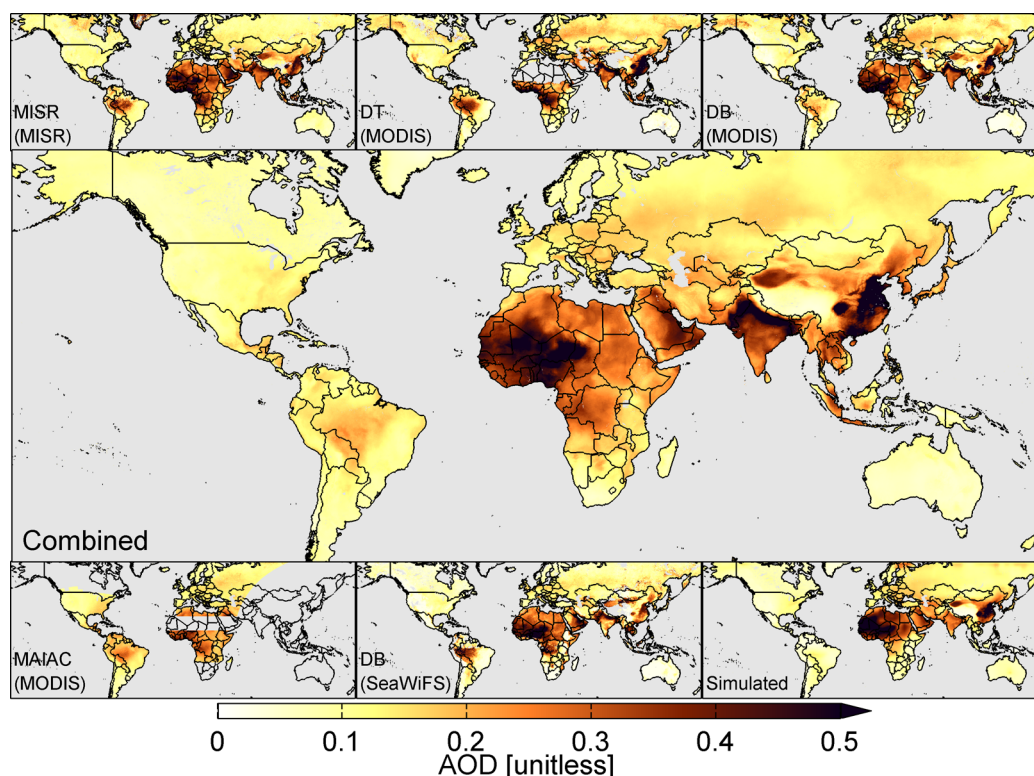


Figure 1. Mean aerosol optical depth (AOD) over land for 2001–2010, by data source. Retrieval algorithm name, where applicable, is given in the lower left of each panel. The associated instrument is indicated in brackets. MODIS corresponds to the average of Aqua- and Terra-based retrievals. The middle panel shows the combination of all data sources after calibrating with AERONET. Gray denotes missing data or water.

were combined using a weighted average, weighted by the product of the inverse residual AOD NRMSD, the inverse absolute percent difference between calibrated and uncalibrated AOD ($\Delta AOD_{adj,n}/AOD_n$), and the local data density ($N_{obs,n}$), such that for AOD:

$$AOD = \frac{\sum_{n=1}^N \frac{1}{NRMSD_n} \times \left(\frac{\Delta AOD_{adj,n}}{AOD_n} \right)^{-1} \times N_{obs,n}^2 \times AOD_n}{\sum_{n=1}^N \frac{1}{NRMSD_n} \times \left(\frac{\Delta AOD_{adj,n}}{AOD_n} \right)^{-1} \times N_{obs,n}^2} \quad (3)$$

$\Delta AOD_{adj,n}$ and AOD_n were set to a minimum of 0.01. N_{obs} was set to a maximum of 5 observations per month for the purpose of weighting, even when more observations were included in the calculation. Squaring N_{obs} penalizes sparse observation density. Values exceeding three standard deviations of those within the surrounding $1^\circ \times 1^\circ$ were replaced via linear interpolation.

Similar weighting was used to combine the monthly $PM_{2.5}$ estimates:

$$SAT PM_{2.5} = \frac{\sum_{n=1}^N \frac{1}{NRMSD_n} \times \left(\frac{\Delta AOD_{adj,n}}{AOD_n} \right)^{-1} \times N_{obs,n}^2 \times PM_{2.5,n}}{\sum_{n=1}^N \frac{1}{NRMSD_n} \times \left(\frac{\Delta AOD_{adj,n}}{AOD_n} \right)^{-1} \times N_{obs,n}^2} \quad (4)$$

Where available, spatial information from the 1 km MAIAC AOD retrieval was then incorporated by applying the climatology of its retrieved relative variation between 0.01° and 0.1° . Where MAIAC was unavailable, monthly AOD and $PM_{2.5}$ were linearly interpolated onto a 0.01° grid.

Global Geographically Weighted Regression (GWR). We predicted and accounted for the bias in the annual mean of these geophysically based $SAT PM_{2.5}$ estimates using GWR.⁴⁶

GWR is a statistical technique that allows spatial variation in the predictor coefficients of a linear regression-based predictor-response relationship, making it possible to predict using the spatial structure of both predictor variables and their coefficients. We fitted our GWR model coefficients at $1^\circ \times 1^\circ$ intervals using $PM_{2.5}$ measured with ground-based monitors (GM), following the form:

$$\begin{aligned} & (GM PM_{2.5} - SAT PM_{2.5}) \\ &= \beta_1 DST + \beta_2 SNAOC + \beta_3 ED \times DU \end{aligned} \quad (5)$$

where β_1 to β_3 represented spatially varying predictor coefficients. ED is the log of the elevation difference between the local elevation and the mean elevation within the simulation grid cell, according to the $1' \times 1'$ ETOPO1 Global Relief Model available from the National Geophysical Data Center (<http://www.ngdc.noaa.gov/mgg/global/seltopo.html>). DU is the inverse distance to the nearest urban land surface, based upon the $1'$ resolution MODIS Land Cover Type Product (MCD12Q1).⁴⁵ Compositional concentrations for mineral dust (DST) and the sum of sulfate, nitrate, ammonium and organic carbon (SNAOC) were represented by simulated relative contributions of each species applied to $SAT PM_{2.5}$, following Philip et al.,⁴² that is, by weighting the near-surface aerosol concentration by the simulated compositional contribution of each species. We interpolated all predictors onto a common 0.01° grid.

The weighting of each ground-based monitor to the local GWR regression was based on the squared inverse distance of the monitor to each GWR grid cell. The greater of 100 km or the third nearest monitor distance was used for the minimum distance to avoid overfitting. We scaled the weighting of

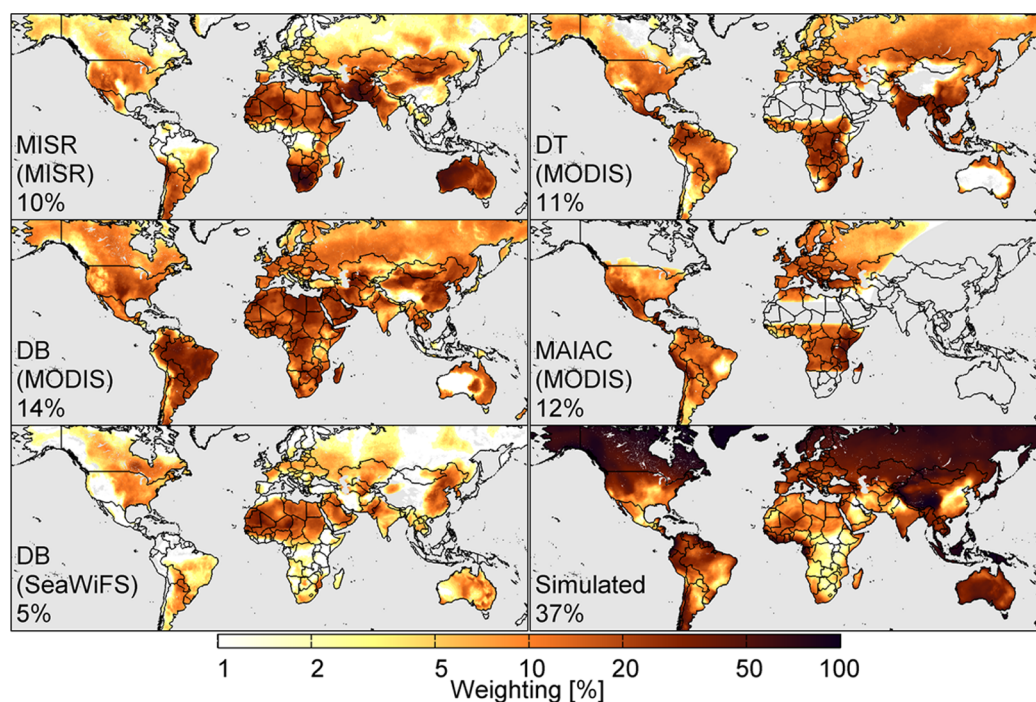


Figure 2. Mean contribution of each data source to the combined $PM_{2.5}$ estimate from 2001 to 2010. Retrieval algorithm name, where applicable, is given in the lower left of each panel. Instrument is indicated in brackets, with average weighting of valid retrievals below. Values in the bottom-left of each panel indicate the decade mean weighting at locations with available data. MODIS corresponds to Terra-based retrievals only. Gray denotes missing data or water. A version with linear color-scale is available as [Supporting Information Figure S3](#).

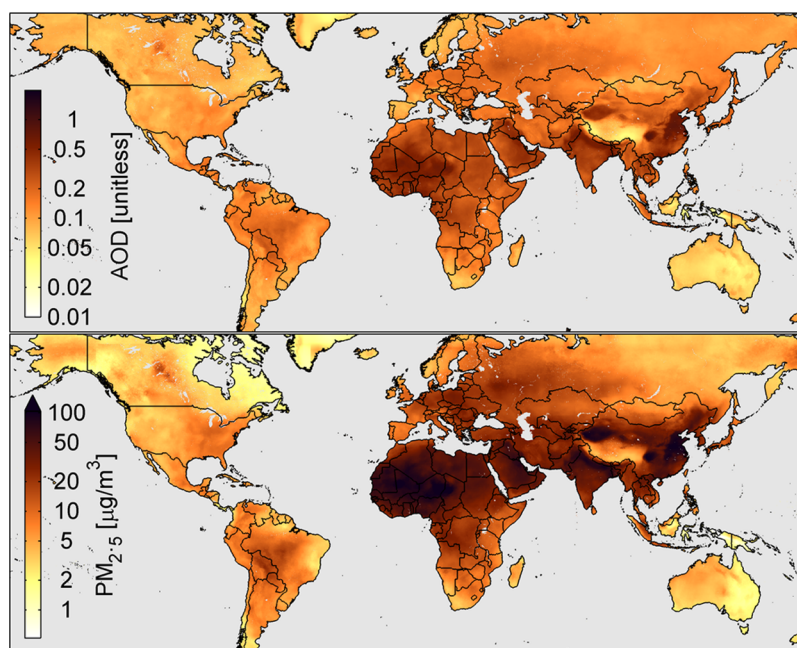


Figure 3. AOD and $PM_{2.5}$ for 2001–2010. The logarithmic $PM_{2.5}$ scale (bottom) is directly proportional to the logarithmic AOD scale, obtained by normalizing the global average of $PM_{2.5}$ to that of AOD. Gray denotes water.

PM_{10} -based observations by half due to uncertainty associated with these values. Ten additional GWR bias corrections were performed for cross validation; each withheld ten percent of sites randomly chosen from within each GBD⁴⁷ defined region ([Supporting Information Figure S2](#)).

We used gridded population estimates at $2.5' \times 2.5'$ resolution from the Socioeconomic Data and Applications Center⁴⁸ for 2010 to further interpret our $PM_{2.5}$ estimates.

4. RESULTS AND DISCUSSION

[Figure 1](#) (top and bottom rows) shows mean AOD from each data source for 2001–2010. A broad level of similarity is apparent across all data sources, with the highest values occurring over regions of dust, biomass burning and anthropogenic activity. Sampling differences affect values in tropical biomass burning regions.

[Figure 2](#) shows mean contributions of each AOD source to the combined product. Aqua- and Terra-based MODIS

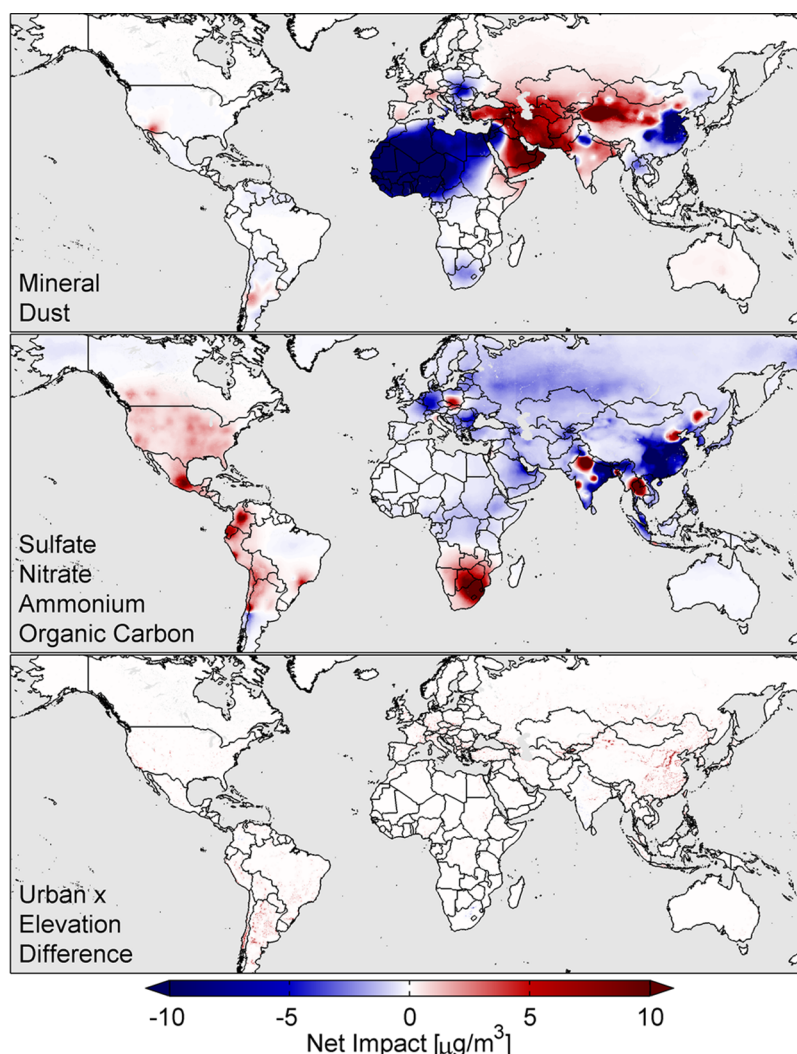


Figure 4. Net impact of individual predictors on the geographically weighted regression estimate of bias in satellite-derived $\text{PM}_{2.5}$ for 2010. Gray denotes water. Percentage impact is plotted in [Supporting Information Figure S4](#).

retrievals were weighted separately, for a total of nine AOD sources, although only Terra-based MODIS retrievals are shown in this figure. An individual source of average quality would therefore have a weighting of $1/9$ ($\sim 10\%$). All sources demonstrated value, excelling under conditions best suited to their individual strengths. The MAIAC and MISR retrievals excelled under difficult surface conditions, such as mountainous and arid regions. MODIS DB was used over broad desert regions, such as the Sahara, and biomass burning regions of South America and Africa. SeaWiFS DB was weighted less heavily, and displayed some similarity to MODIS DB, but reduced in part by less frequent sampling. DT was used in the vegetatively rich regions of Central America, Central Africa, and Southeast Asia. Simulated AOD was highly valuable in northern regions, where seasonal snow-cover inhibit passive AOD retrieval, and in tropical southeastern Asia, where cirrus cloud-cover reduces satellite sampling. Combined AOD is more consistent than individual AOD data sources at sites with ground-based measurements of $\text{PM}_{2.5}$ ($r^2 = 0.32\text{--}0.39$ vs $r^2 = 0.45$) and at sites that also include $\text{PM}_{2.5}$ estimated from PM_{10} ($r^2 = 0.35\text{--}0.42$ vs $r^2 = 0.49$).

Figure 1 (middle) shows the combined 2001–2010 multi-year mean AOD. The top panel of **Figure 3** shows the same

data on a logarithmic scale proportional to the $\text{PM}_{2.5}$ estimates shown in the bottom panel. The two logarithmic color scales differ by a factor of $52 \mu\text{g}/\text{m}^3$, equal to the global average simulated ratio of $\text{PM}_{2.5}$ to AOD. Relative differences in spatial variation represent deviations from global mean conditions of the aerosol vertical profile and optical properties. Source regions, such as deserts and industrial areas, show greater $\text{PM}_{2.5}$ values compared to AOD reflecting enhanced near-surface aerosol concentrations. Northern regions tend to have less surface $\text{PM}_{2.5}$ compared to aerosol aloft.

Figure 4 shows the net impact of individual predictors on the GWR bias correction to the annual mean $\text{PM}_{2.5}$ estimates. Urban Distance \times Elevation Difference shows the largest amount of spatial heterogeneity owing to predictor variation. $\text{PM}_{2.5}$ components are associated with large scale changes that likely represent bias in the AOD to $\text{PM}_{2.5}$ relationship rather than bias in AOD since AOD was calibrated with AERONET. Mineral Dust is regionally associated with both reductions and enhancements, potentially tied to variability in the simulated accuracy of wet deposition⁴¹ that may affect the accuracy of simulated composition. Bias associated with other $\text{PM}_{2.5}$ components shows more variation, including reductions over parts of East Asia and Eastern Europe, and increases around

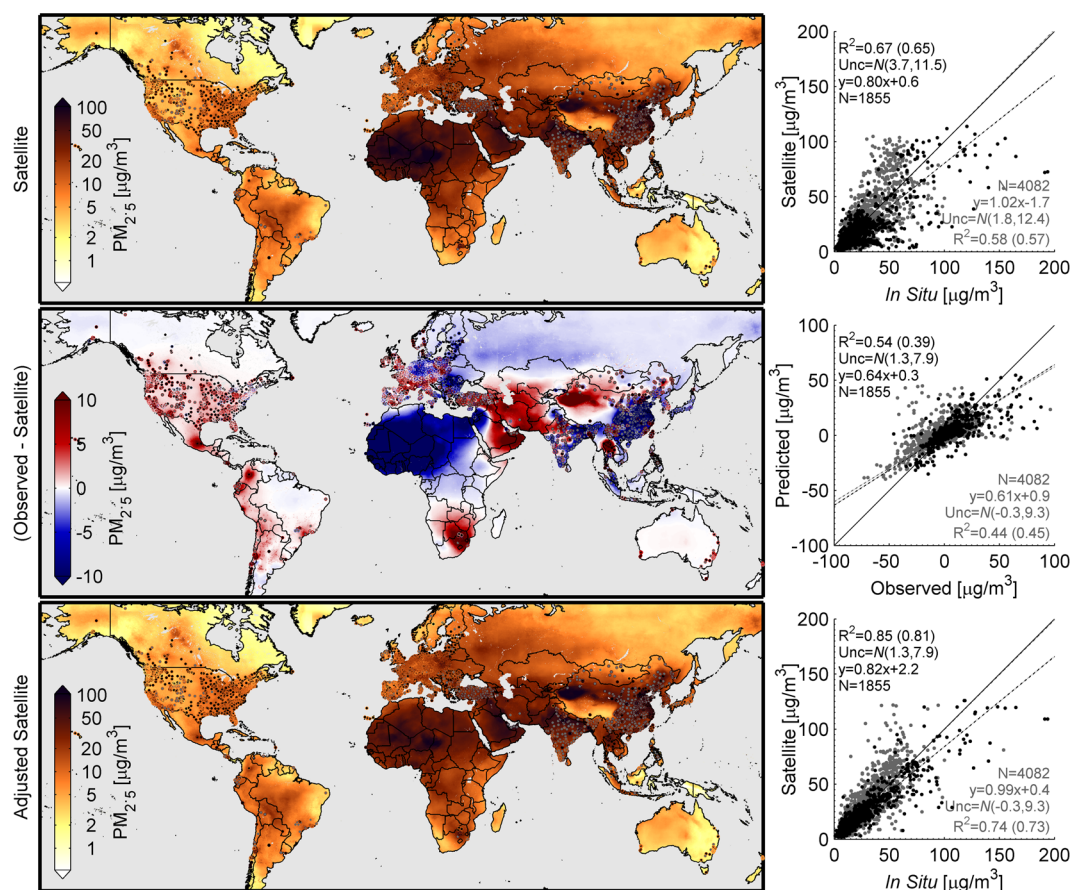


Figure 5. Satellite-derived PM_{2.5} (top), predicted bias (middle), and adjusted satellite-derived PM_{2.5} (bottom) for 2010. In situ values are for the year of observation of each monitor, with years between 2008 and 2013. Point locations correspond to individual monitors, with black dots representing direct PM_{2.5} observations and gray dots representing PM_{2.5} approximated from PM₁₀. Colored outlines of point locations provide observed value. Gray space denotes water. The right column plots coincident annual mean in situ and satellite values. Annotations include the coefficient of variation at all points and at cross-validation points (R^2 = All points (CV points)), normal distribution of uncertainty ($N(\text{bias}, \text{variance})$), line of best fit (y) and number of comparison points (N). Black dots/text correspond to direct PM_{2.5} monitors alone. Gray dots and text additionally include PM_{2.5} estimated from PM₁₀ monitors.

some cities especially in South America and western North America.

Figure 5 (middle) shows the combined impact of all predictors on the annual mean geophysically based satellite-derived PM_{2.5} for 2010. Changes associated with mineral dust remained prevalent, overlaid with regional changes associated with other composition components. Fine scale variability (Supporting Information Figure S5) is associated with Elevation and Urban Distance. Agreement between the GWR-Predicted and Observed bias was weaker when including PM₁₀-based values ($R^2 = 0.44$) versus those sites directly measuring PM_{2.5} ($R^2 = 0.54$). A slope of 0.6 suggests that the net bias may be underestimated.

Figure 5 also shows comparisons of ground monitors with initial, annual mean geophysically based satellite-derived PM_{2.5} (top) and GWR-adjusted satellite-derived PM_{2.5} (bottom). Addition of the predicted bias significantly improves agreement with both the entire in situ data set ($R^2 = 0.74$ vs $R^2 = 0.58$) and with the direct PM_{2.5} observations ($R^2 = 0.85$ vs $R^2 = 0.67$). Agreement of the GWR-adjusted estimates at cross validation sites was similar when including PM₁₀-based monitors ($R^2 = 0.73$) and at the direct PM_{2.5} locations ($R^2 = 0.81$), suggesting the impact of overfitting is small. Comparison between these annual mean values include any residual impact of sampling. The weaker overall relationship with PM_{2.5}

inferred from PM₁₀ may suggest caution in the use of PM₁₀ for PM_{2.5} exposure estimates, or alternatively the higher density of PM₁₀ monitors in more uncertain regions, such as India.

Table 1 gives mean population-weighted PM_{2.5} concentration for the socioeconomic-geographic regions of GBD. The larger global population-weighted mean PM_{2.5} concentration (32.6 μg/m³) compared with that at PM_{2.5} monitor locations (25.1 μg/m³) highlights the need for additional monitoring. Regional differences between the GWR-adjusted and prior GBD2013 estimates are apparent, with a root-mean-square difference of regional mean GWR-adjusted values at PM_{2.5}-monitor locations of 7.0 μg/m³ versus 12.8 μg/m³ for the GBD2013 estimates. North America, Central Europe and Eastern Europe have low levels of within-region uncertainty compared to PM_{2.5} monitors (bias: −0.7 to 0.4 μg/m³, variance: 2.1–5.7 μg/m³), benefiting from well-characterized emission inventories that drive AOD to PM_{2.5} relationships as well as numerous ground-based monitors for GWR adjustment. Parts of Asia and Latin America, by contrast, have relatively high levels of regional uncertainty (bias: up to 11.6 μg/m³, variance: up to 33.9 μg/m³). This increased absolute uncertainty results in part from the higher PM_{2.5} concentrations in many Asian regions. Lower in situ monitor density may also play a role, suggesting increased uncertainty in GWR-adjusted values for sparsely observed regions.

Table 1. Population-Weighted Mean $PM_{2.5}$ ($\mu g/m^3$) by Global Burden of Disease (GBD) Region^b, Satellite (SAT), GWR-Adjusted Satellite (GWR SAT) for 2010^a

region	population [million people]	at PM _{2.5} monitor locations					at PM _{2.5} and PM ₁₀ monitor locations									
		SAT PM _{2.5}	GWR SAT PM _{2.5}	GBD ^c PM _{2.5}	dust [%]		SAT PM _{2.5}	GWR SAT PM _{2.5}	GBD ^c PM _{2.5}	in situ PM _{2.5}	N [#]	SAT PM _{2.5}	GWR SAT PM _{2.5}	GBD ^c PM _{2.5}	in situ PM _{2.5}	N [#]
Global	6309	36.3	32.6	31.3	25		20.8 (3.7,11.5)	25.1 (1.3,7.9)	24.0 (2.2,11.4)	26.5	1854	23.9 (1.8,12.4)	27.2 (−0.3,9.3)	27.9 (1.1,12.1)	26.6	4079
Asia Pacific, High Income	169	17.6	16.9	20.2	18		17.1 (4.1,3.4)	18.9 (1.7,3.5)	22.5 (−0.3,6.1)	20.1	11	21.0 (−0.5,3.9)	22.3 (−1.7,4.1)	26.0 (−3.2,5.4)	20.3	68
Asia, Central	79	25.9	29.4	21.8	65		10.0 (8.6,25.8)	31.6 (3.2,16.4)	13.2 (−5.3,33.1)	47.3	8	8.0 (16.0,21.4)	31.6 (7.9,16.2)	10.3 (9.6,27.9)	43.1	18
Asia, East	1363	59.8	46.6	53.0	17		59.8 (11.3,28.3)	61.5 (11.6,19.1)	59.1 (14.9,22.2)	72.1	97	60.9 (−4.4,25.3)	60.0 (−3.5,17.9)	60.3 (−2.1,21.8)	57.5	401
Asia, South	1545	52.3	50.6	43.1	22		58.3 (29.1,36.1)	77.8 (8.9,33.9)	55.2 (36.8,36.7)	80.2	18	49.1 (−2.6,22.3)	55.3 (−6.5,20.6)	49.3 (−2.1,23.0)	51.4	203
Asia, Southeast	575	17.1	17.2	16.2	5		21.4 (18.8,16.4)	26.0 (6.0,15.9)	21.9 (19.9,17.0)	27.2	62	23.0 (8.4,18.8)	26.3 (0.9,15.4)	25.0 (8.4,20.2)	25.2	117
Australasia	23	2.5	4.1	7.0	17		2.4 (3.9,1.5)	5.9 (1.3,2.2)	8.2 (−0.6,2.8)	6.1	44	2.4 (3.7,1.3)	5.8 (1.2,2.0)	8.4 (−0.9,2.6)	6.0	70
Caribbean	33	5.4	5.7	10.4	34						0	4.9 (−,−)	8.5 (−,−)	10.2 (−,−)	18.0	1
Europe, Central	119	23.3	21.9	17.5	29		25.1 (0.3,8.7)	25.5 (−0.7,5.7)	18.9 (6.5,7.6)	25.3	166	24.0 (0.4,8.5)	25.1 (−0.7,6.6)	18.7 (6.4,7.9)	24.8	511
Europe, Eastern	199	19.2	18.1	14.6	30		11.1 (−2.2,6.5)	10.5 (−0.9,5.6)	14.7 (−3.0,7.2)	9.6	26	13.2 (−2.3,6.1)	12.3 (−1.1,5.4)	14.6 (−2.4,6.9)	11.3	31
Europe, Western	380	14.7	13.7	15.2	19		15.1 (0.7,5.1)	15.9 (0.4,3.3)	17.1 (−0.3,4.0)	16.5	535	14.7 (0.8,5.1)	15.9 (0.1,3.7)	17.0 (−0.3,4.3)	16.1	1307
Latin America, Andean	52	8.3	15.1	10.7	1		9.0 (28.6,15.7)	33.6 (3.6,11.3)	21.2 (17.3,13.5)	41.9	4	8.1 (15.9,12.6)	27.1 (4.9,9.5)	17.7 (12.1,11.0)	34.7	16
Latin America, Central	231	6.8	10.8	12.1	12		8.4 (14.8,5.3)	18.1 (5.9,8.1)	17.1 (8.9,6.6)	22.5	17	8.0 (13.4,5.0)	16.7 (4.5,7.5)	16.0 (7.6,5.3)	21.3	41
Latin America, Southern	60	6.6	10.9	11.9	37		8.5 (28.5,22.8)	25.0 (6.2,15.5)	31.5 (17.5,30.1)	29.6	29	8.4 (20.5,19.9)	20.0 (2.9,14.8)	23.6 (12.4,23.8)	25.4	52
Latin America, Tropical	189	6.8	9.0	14.1	3		8.5 (7.0,5.6)	16.1 (−0.2,5.0)	28.5 (−9.8,7.1)	17.0	19	8.6 (6.0,5.0)	14.6 (0.1,4.5)	35.7 (−10.9,10.2)	15.5	72
North Africa/ Middle East	432	30.0	30.2	29.0	81		30.7 (6.3,16.6)	38.4 (−0.8,16.0)	43.0 (1.0,14.0)	37.5	8	29.7 (9.3,14.2)	38.0 (2.6,12.0)	40.7 (15.1,17.2)	34.9	117
North America, High Income	326	7.4	9.2	11.8	7		7.9 (2.3,2.5)	10.0 (0.4,2.1)	13.8 (−1.1,3.5)	10.1	791	7.6 (2.8,3.2)	10.0 (0.8,2.8)	13.4 (−0.5,3.9)	10.2	1020
Oceania	6	1.6	1.6	5.5	0						0					0
Sub-Saharan Africa, Central	99	21.9	21.5	15.6	9						0					0
Sub-Saharan Africa, East	335	16.6	16.2	13.7	30						0					0
Sub-Saharan Africa, Southern	66	8.5	19.0	12.5	10		10.8 (21.8,14.7)	36.6 (−0.6,10.2)	19.3 (15.9,11.3)	40.2	14	10.5 (23.8,17.3)	34.7 (2.5,14.4)	21.5 (16.1,14.7)	52.3	29
Sub-Saharan Africa, West	315	57.1	39.5	27.7	73		60.7 (−25.8,6.6)	47.4 (−10.6,11.3)	33.1 (2.8,3.9)	33.0	5	60.7 (−25.8,6.6)	47.4 (−10.6,11.3)	33.1 (2.8,3.9)	33.0	5

^aBracketed terms provide the regional normal distribution of uncertainty ($N(\text{bias}, \text{variance})$) compared to local in situ observations. ^bLim et al., 2012;⁴⁷ Figure S1. ^cBrauer et al., 2016.²

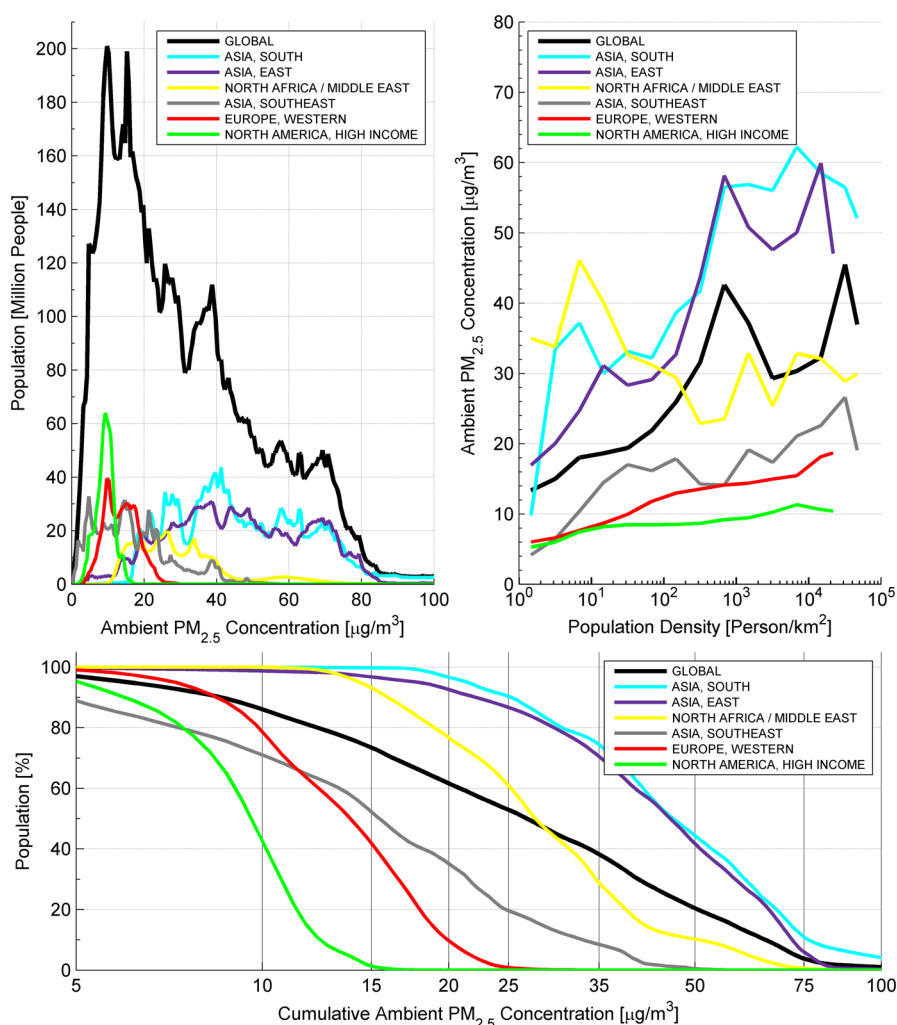


Figure 6. Distribution of GWR-adjusted satellite-derived $\text{PM}_{2.5}$ concentration for 2010 according to population and population density within the six most populated GBD regions and globally. The bottom panel shows the cumulative distribution of regional, annual mean $\text{PM}_{2.5}$.

According to the GWR-adjusted satellite-derived $\text{PM}_{2.5}$ estimates, the global population-weighted annual average $\text{PM}_{2.5}$ concentration of $32.6 \mu\text{g}/\text{m}^3$ is three times higher than the $10 \mu\text{g}/\text{m}^3$ WHO guideline, driven by high concentrations in several Asian and African regions. Few regions have population-weighted mean concentrations below the WHO guideline, with only Australasia, the Caribbean, Tropical Latin America, High Income North America, and Oceania below this level. South and East Asia contain the highest population-weighted $\text{PM}_{2.5}$ concentrations ($50.6 \mu\text{g}/\text{m}^3$ and $46.6 \mu\text{g}/\text{m}^3$, respectively), influenced by both mineral dust and anthropogenic emissions. West Sub-Saharan Africa also had high population-weighted $\text{PM}_{2.5}$ concentrations ($39.5 \mu\text{g}/\text{m}^3$), due to the combined effects of mineral dust and biomass burning.

Figure 6 shows the distribution of GWR-adjusted satellite-derived $\text{PM}_{2.5}$ concentrations for 2010 according to population and population density for the six most populated GBD regions and globally. Typical ambient concentrations in South Asia and East Asia vary, from about $20\text{--}70 \mu\text{g}/\text{m}^3$. North Africa/Middle East uniquely had its highest $\text{PM}_{2.5}$ concentrations in its least populated regions due to substantial mineral dust concentrations near the sparsely populated Sahara Desert. Average $\text{PM}_{2.5}$ concentrations in the least densely populated regions of South Asia and East Asia exceeded those in the most densely populated regions of North America. A small proportion of the

global population (13%) lived where concentrations are below the $10 \mu\text{g}/\text{m}^3$ WHO guideline. Regionally, 52% of the High Income North America population live below the WHO guideline, compared to 1% or less of South Asia, East Asia, and North Africa/Middle East.

Next Steps. Here we presented a globally applicable method that brought together satellite retrievals, geophysically driven simulations, and ground-based observations to improve the representation of $\text{PM}_{2.5}$ at spatial scales commensurate with population density. Eight different satellite AOD products were combined for broad global accuracy at 0.1° resolution. Information at 0.01° was obtained from the MAIAC retrieval and from the associations of $\text{PM}_{2.5}$ enhancements with topographic depressions. These multiple information sources enabled predictive skill worldwide despite a dearth of ground-based monitors outside High Income North America, Western Europe, and recently, China. A more integrated ground-based $\text{PM}_{2.5}$ and AOD monitoring strategy, such as the Surface Particulate Matter Network (SPARTAN),⁴⁹ would offer value for independent evaluation of the AOD-to- $\text{PM}_{2.5}$ relationship. Higher temporal availability of global $\text{PM}_{2.5}$ monitors would allow better GWR representation of seasonally driven bias, such as that associated with mineral dust and biomass burning. Regions heavily influenced by mineral dust present a challenge for satellite retrievals, simulation, and

ground measurements. Future simulations should incorporate improved dust emission schemes (e.g., Ridley et al.⁴¹) to reduce uncertainty. Higher resolution simulations may also better represent finer-scale features of the geophysically based AOD to PM_{2.5} relationship. The approach presented here allows for future evaluation and inclusion of numerous AOD retrievals, such as from emerging high-resolution products (e.g., Visible Infrared Radiometer Suite (VIIRS),⁵⁰ 3 km MODIS DT⁵¹), as well as the inclusion of additional ground-based observations as they become available. Alternative statistical calibration methods, such as a Bayesian Hierarchical Framework,^{52,53} may offer additional benefits.

The annual mean global GWR-adjusted PM_{2.5} estimates at 0.01° × 0.01° are freely available as a public good from the Dalhousie University Atmospheric Composition Analysis Group Web site at: http://fizz.phys.dal.ca/~atmos/martin/?page_id=140, or by contacting the authors.

■ ASSOCIATED CONTENT

● Supporting Information

The Supporting Information is available free of charge on the ACS Publications website at DOI: 10.1021/acs.est.5b05833.

Additional information as noted in the text (PDF)

■ AUTHOR INFORMATION

Corresponding Author

*Phone: (902) 494-1820; e-mail: Aaron.van.Donkelaar@dal.ca.

Notes

The authors declare no competing financial interest.

■ ACKNOWLEDGMENTS

We are grateful to the MODIS, MISR, SeaWiFS, CALIOP, and AERONET teams that have made this work possible through the creation, validation, and public release of their data products, as well as Compute Canada for computing resources. This work was supported by the Natural Science and Engineering Research Council of Canada. SeaWiFS and MODIS Deep Blue data set development was supported by the NASA MEaSUREs and EOS programs, respectively.

■ REFERENCES

- (1) Forouzanfar, M. H.; Alexander, L.; Anderson, H. R.; Bachman, V. F.; Biryukov, S.; et al. Global, regional, and national comparative risk assessment of 79 behavioural, environmental and occupational, and metabolic risks or clusters of risks in 188 countries, 1990–2013: a systematic analysis for the Global Burden of Disease Study 2013. *Lancet* **2015**, *386* (10010), 2287–2323.
- (2) Brauer, M.; Freedman, G.; Frostad, J. J.; van Donkelaar, A.; Martin, R. V.; et al. Ambient air pollution exposure estimation for the global burden of disease 2013. *Environ. Sci. Technol.* **2016**, *50* (1), 79–88.
- (3) van Donkelaar, A.; Martin, R. V.; Brauer, M.; Boys, B. L. Use of Satellite Observations for Long-Term Exposure Assessment of Global Concentrations of Fine Particulate Matter. *Environ. Health Perspect.* **2015**, *123* (2), 135–143.
- (4) Kloog, I.; Chudnovsky, A. A.; Just, A. C.; Nordio, F.; Koutrakis, P.; et al. A new hybrid spatio-temporal model for estimating daily multi-year PM_{2.5} concentrations across northeastern USA using high resolution aerosol optical depth data. *Atmos. Environ.* **2014**, *95*, 581–590.
- (5) Ma, Z.; Hu, X.; Huang, L.; Bi, J.; Liu, Y. Estimating ground-level PM_{2.5} in China using satellite remote sensing. *Environ. Sci. Technol.* **2014**, *48* (13), 7436–7444.
- (6) Vinneau, D.; de Hoogh, K.; Bechle, M. J.; Beelen, R.; van Donkelaar, A.; et al. Western European land use regression incorporating satellite- and ground-based measurements of NO₂ and PM₁₀. *Environ. Sci. Technol.* **2013**, *47* (23), 13555–13564.
- (7) Levy, R. C.; Mattoo, S.; Munchak, L. A.; Remer, L. A.; Sayer, A. M.; et al. The Collection 6 MODIS aerosol products over land and ocean. *Atmos. Meas. Tech.* **2013**, *6*, 2989–3034.
- (8) Levy, R. C.; Remer, L. A.; Mattoo, S.; Vermote, E. F.; Kaufman, Y. J. Second-generation operational algorithm: Retrieval of aerosol properties over land from inversion of Moderate Resolution Imaging Spectroradiometer spectral reflectance. *J. Geophys. Res.* **2007**, *112* (D13), n/a10.1029/2006JD007811
- (9) Hsu, N. C.; Jeong, M. J.; Bettenhausen, C.; Sayer, A. M.; Hansell, R.; et al. Enhanced Deep Blue aerosol retrieval algorithm: The second generation. *J. Geophys. Res.* **2013**, *118*, 1–20.
- (10) Hsu, N. C.; Tsay, S. C.; King, M. D.; Herman, J. R. Deep blue retrievals of Asian aerosol properties during ACE-Asia. *IEEE T. Geosci. Remote* **2006**, *44* (11), 3180–3195.
- (11) Lyapustin, A.; Martonchik, J.; Wang, Y. J.; Laszlo, I.; Korkin, S. Multiangle implementation of atmospheric correction (MAIAC): 1. Radiative transfer basis and look-up tables. *J. Geophys. Res.* **2011**, *116*.10.1029/2010JD014985
- (12) Lyapustin, A.; Wang, Y.; Laszlo, I.; Kahn, R.; Korkin, S., et al. Multiangle implementation of atmospheric correction (MAIAC): 2. Aerosol algorithm. *J. Geophys. Res.* **2011**, *116*.10.1029/2010JD014986
- (13) Kahn, R. A.; Gaitley, B. J. An analysis of global aerosol type as retrieved by MISR. *J. Geophys. Res., Atmos.* **2015**, *120*.424810.1002/2015JD023322
- (14) Holben, B. N.; Eck, T. F.; Slutsker, I.; Tanre, D.; Buis, J. P.; et al. AERONET - A federated instrument network and data archive for aerosol characterization. *Remote Sens. Environ.* **1998**, *66* (1), 1–16.
- (15) van Donkelaar, A.; Martin, R. V.; Spurr, R. J. D.; Burnett, R. T. High-resolution satellite-derived PM_{2.5} from optimal estimation and geographically weighted regression over North America. *Environ. Sci. Technol.* **2015**, *49* (17), 10482–10491.
- (16) Winker, D. M.; Vaughan, M. A.; Omar, A.; Hu, Y.; Powell, K. A. Overview of the CALIPSO mission and CALIOP data processing algorithms. *Journal of Atmospheric and Oceanic Technology* **2009**, *26*, 2310–2323.
- (17) Levy, R. C.; Munchak, L. A.; Mattoo, S.; Patadia, F.; Remer, L. A.; et al. Towards a long-term global aerosol optical depth record: applying a consistent aerosol retrieval algorithm to MODIS and VIIRS-observed reflectance. *Atmos. Meas. Tech.* **2015**, *8*, 4083–4110.
- (18) Zhang, J.; Reid, J. S. A decadal regional and global trend analysis of the aerosol optical depth using a data-assimilation grade over-water MODIS and Level 2 MISR aerosol products. *Atmos. Chem. Phys.* **2010**, *10*, 10949–10963.
- (19) Bruegge, C. J.; Diner, D. J.; Kahn, R. A.; Chrien, N.; Helmlinger, M. C.; et al. The MISR radiometric calibration process. *Remote Sens. Environ.* **2007**, *107*, 2–11.
- (20) Eplee, R. E.; Meister, G.; Patt, F. S.; Franz, B. A.; McClain, C. R., Uncertainty Assessment of the SeaWiFS On-Orbit Calibration. In *Earth Observing Systems XVI*; Butler, J. J., Xiong, X., Gu, X., Eds.; Proc. of SPIE, 2011; Vol. 8153, p 815310.
- (21) Sayer, A. M.; Munchak, L. A.; Hsu, N. C.; Levy, R. C.; Bettenhausen, C.; et al. MODIS Collection 6 aerosol products: Comparison between Aqua's e-Deep Blue, Dark Target, and "merged" data sets, and usage recommendations. *Journal of Geophysical Research: Atmospheres* **2014**, *119*, 13,965–13,989.
- (22) Petrenko, M.; Ichoku, C. Coherent uncertainty analysis of aerosol measurements from multiple satellite sensors. *Atmos. Chem. Phys.* **2013**, *13*, 6777–6805.
- (23) Sayer, A. M.; Hsu, N. C.; Bettenhausen, C.; Jeong, M.-J.; Zhang, J. Global and regional evaluation of over-land spectral aerosol optical depth retrievals from SeaWiFS. *Atmos. Meas. Tech.* **2012**, *5*, 1761–1778.
- (24) Martonchik, J. V.; Kahn, R. A.; Diner, D. J., Retrieval of Aerosol Properties over Land Using MISR Observations. In *Satellite Aerosol*

Remote Sensing Over Land; Kokhanovsky, A. A.; Leeuw, G. d., Eds.; Springer: Berlin, 2009; pp 267–293.

(25) Zhang, L.; Jacob, D. J.; Knipping, E. M.; Kumar, N.; Munger, J. W.; et al. Nitrogen deposition to the United States: distribution, sources, and processes. *Atmos. Chem. Phys.* **2012**, *12*, 4539–4554.

(26) van Donkelaar, A.; Martin, R. V.; Pasch, A. N.; Szykman, J. J.; Zhang, L.; et al. Improving the accuracy of daily satellite-derived ground-level fine aerosol concentration estimates for North America. *Environ. Sci. Technol.* **2012**, *46*, 11971–11978.

(27) van Donkelaar, A.; Martin, R. V.; Spurr, R. J. D.; Drury, E.; Remer, L. A.; et al. Optimal estimation for global ground-level fine particulate matter concentrations. *J. Geophys. Res.* **2013**, *118*, 1–16.

(28) Chen, D.; Wang, X. T.; McElroy, M. B.; He, K.; Yantosca, R. M.; et al. Regional CO pollution in China simulated by the high-resolution nested-grid GEOS-Chem model. *Atmos. Chem. Phys.* **2009**, *9*, 3825–3839.

(29) Park, R. J.; Jacob, D. J.; Field, B. D.; Yantosca, R. M.; Chin, M. Natural and transboundary pollution influences on sulfate-nitrate-ammonium aerosols in the United States: Implications for policy. *J. Geophys. Res.* **2004**, *109* (D15).[10.1029/2003JD004473](https://doi.org/10.1029/2003JD004473)

(30) Pye, H. O. T.; Liao, H.; Wu, S.; Mickley, L. J.; Jacob, D. J., et al. Effect of changes in climate and emissions on future sulfate-nitrate-ammonium aerosol levels in the United States. *J. Geophys. Res.* **2009**, *114*(D01205).[10.1029/2008JD010701](https://doi.org/10.1029/2008JD010701)

(31) Heald, C. L.; Coe, H.; Jimenez, J. L.; Weber, R. J.; Bahreini, R.; et al. Exploring the vertical profile of atmospheric organic aerosol: comparing 17 aircraft field campaigns with a global model. *Atmos. Chem. Phys.* **2011**, *11*, 12673–12696.

(32) Park, R. J.; Jacob, D. J.; Chin, M.; Martin, R. V. Sources of carbonaceous aerosols over the United States and implications for natural visibility. *J. Geophys. Res.* **2003**, *108* (D12).[10.1029/2002JD003190](https://doi.org/10.1029/2002JD003190)

(33) Wang, Q.; Jacob, D. J.; Fisher, J. A.; Mao, J. T.; Leibensperger, E. M.; et al. Sources of carbonaceous aerosol and deposited black carbon in the Arctic in winter-spring: implications for radiative forcing. *Atmos. Chem. Phys.* **2011**, *11*, 12453–12473.

(34) Liao, H.; Henze, D. K.; Seinfeld, J. H.; Wu, S. L.; Mickley, L. J. Biogenic secondary organic aerosol over the United States: Comparison of climatological simulations with observations. *J. Geophys. Res.* **2007**, *112* (D6).[10.1029/2006JD007813](https://doi.org/10.1029/2006JD007813)

(35) Henze, D. K.; Seinfeld, J. H. Global secondary organic aerosol from isoprene oxidation. *Geophys. Res. Lett.* **2006**, *33* (9).[10.1029/2006GL025976](https://doi.org/10.1029/2006GL025976)

(36) Henze, D. K.; Seinfeld, J. H.; Ng, N. L.; Kroll, J. H.; Fu, T. M.; et al. Global modeling of secondary organic aerosol formation from aromatic hydrocarbons: high- vs. low-yield pathways. *Atmos. Chem. Phys.* **2008**, *8*, 2405–2421.

(37) Fairlie, T. D.; Jacob, D. J.; Park, R. J. The impact of transpacific transport of mineral dust in the United States. *Atmos. Environ.* **2007**, *41* (6), 1251–1266.

(38) Jaegle, L.; Quinn, P. K.; Bates, T.; Alexander, B.; Lin, J.-T. Global distribution of seas salt aerosols: New constraints from in situ and remote sensing observations. *Atmos. Chem. Phys.* **2011**, *11*, 3137–3157.

(39) Martin, R. V.; Jacob, D. J.; Yantosca, R. M.; Chin, M.; Ginoux, P. Global and regional decreases in tropospheric oxidants from photochemical effects of aerosols. *J. Geophys. Res.* **2003**, *108* (D3).[10.1029/2002JD002622](https://doi.org/10.1029/2002JD002622)

(40) Drury, E.; Jacob, D. J.; Wang, J.; Spurr, R. J. D.; Chance, K. Improved algorithm for MODIS satellite retrievals of aerosol optical depths over western North America. *J. Geophys. Res.* **2008**, *113* (D16).[10.1029/2007JD009573](https://doi.org/10.1029/2007JD009573)

(41) Ridley, D. A.; Heald, C. L.; Ford, B. J. North African dust export and deposition: A satellite and model perspective. *J. Geophys. Res.* **2012**, *117* (D02202). [10.1029/2011JD016794](https://doi.org/10.1029/2011JD016794)

(42) Philip, S.; Martin, R. V.; Van Donkelaar, A.; Lo, J. W.-H.; Wang, Y.; et al. Global chemical composition of ambient fine particulate matter for exposure assessment. *Environ. Sci. Technol.* **2014**, *48*, 13060–13068.

(43) Boys, B.; Martin, R. V.; Van Donkelaar, A.; MacDonell, R.; Hsu, N. C.; et al. Fifteen year global time series of satellite-derived fine particulate matter. *Environ. Sci. Technol.* **2014**, *48*, 11109–11118.

(44) Holben, B. N.; Tanre, D.; Smirnov, A.; Eck, T. F.; Slutsker, I.; et al. An emerging ground-based aerosol climatology: Aerosol optical depth from AERONET. *J. Geophys. Res.* **2001**, *106* (D11), 12067–12097.

(45) Freidl, M. A.; Sulla-Menashe, D.; Tan, B.; Schneider, A.; Ramankutty, N.; et al. MODIS Collection 5 global land cover: Algorithm refinements and characterization of new datasets. *Remote Sens. Environ.* **2010**, *114*, 168–182.

(46) Brunson, C.; Fotheringham, A. S.; Charlton, M. E. Geographically Weighted Regression: A method for exploring spatial nonstationarity. *Geographic Analysis* **1996**, *28* (4), 281–298.

(47) Lim, S. S.; Vos, T.; Flaxman, A. D. F.; Danaei, G.; Shibuya, K.; et al. A comparative risk assessment of burden of disease and injury attributable to 67 risk factors and risk factor clusters in 21 regions, 1990–2010: a systematic analysis for the Global Burden of Disease Study 2010. *Lancet* **2012**, *380*, 2224–2260.

(48) CEISIN (Center for International Earth Science Information Network) Gridded Population of the World, Version 3 (GPWv3). In NASA Socioeconomic Data and Applications Center (SEDAC) 2005. <http://sedac.ciesin.columbia.edu/data/collection/gpw-v3>.

(49) Snider, G. C.; Weagle, C. L.; Martin, R. V.; Van Donkelaar, A.; Conrad, K.; et al. SPARTAN: A Global Network to Evaluate and Enhance Satellite-Based Estimates of Ground-Level Particulate Matter for Global Health Applications. *Atmos. Meas. Tech.* **2015**, *8*, 505–521.

(50) Justice, C. O.; Román, M. O.; Csizsar, I.; Vermote, E. F.; Wolfe, R. E.; et al. Land and cryosphere products from Suomi NPP VIIRS: Overview and status. *Journal of Geophysical Research: Atmospheres* **2013**, *118* (17), 9753–9765.

(51) Remer, L. A.; Mattoo, S.; Levy, R. C.; Munchak, L. A. MODIS 3 km aerosol product: algorithm and global perspective. *Atmos. Meas. Tech.* **2013**, *6*, 1829–1844.

(52) Shaddick, G.; Zidek, J. V. A case study in preferential sampling: Long term monitoring of air pollution in the UK. *Spatial Statistics* **2014**, *9*, 51–65.

(53) Cameletti, M.; Lindgren, F.; Simpson, D.; Rue, H. Spatio-temporal modeling of particulate matter concentration through the SPDE approach. *ASTA Advances in Statistical Analysis* **2013**, *97* (2), 109–131.